

HYDROGEN PRODUCTION THROUGH REFORMING OF BIOGAS

Acceptance date: 01/12/2023

André Luiz Alvarenga Marinho

Federal University of Rio de Janeiro,
Chemical Engineering Program of
COPPE/UFRJ, Rio de Janeiro, Brazil
National Institute of Technology, Division
of Catalysis, Biocatalysis and Process, Rio
de Janeiro, Brazil

Raimundo Crisóstomo Rabelo-Neto

National Institute of Technology, Division
of Catalysis, Biocatalysis and Process, Rio
de Janeiro, Brazil

Fabio Souza Toniolo

Federal University of Rio de Janeiro,
Chemical Engineering Program of
COPPE/UFRJ, Rio de Janeiro, Brazil

Fabio Bellot Noronha

National Institute of Technology, Division
of Catalysis, Biocatalysis and Process, Rio
de Janeiro, Brazil
University of Lille, CNRS, Centrale Lille,
ENSCL, Univ. Artois, UMR 8181—UCCS—
Unité de Catalyse et Chimie du Solide,
59000 Lille, France

ABSTRACT: Biogas has great potential for the production of renewable hydrogen via dry reforming of methane. The primary challenge of this technology is catalyst

deactivation, mainly through carbon deposition. In this review, the mechanism of carbon formation is presented, and the different strategies for minimizing carbon deposition are discussed, which include (i) controlling the size of the metallic crystallite and (ii) the use of supports with redox properties. Selection of the catalyst preparation method is essential to control the size of the metallic particles and, consequently, the stability of the catalysts in the dry reforming of methane reaction. Another approach consists of increasing the carbon gasification rate by using supports with high oxygen mobility, based on the role of support in the mechanism of dry reforming of methane reaction. Different examples of catalyst design are discussed involving various preparation methods, such as core-shell, perovskite-type oxide, and spinel phase, to develop a catalyst resistant to carbon deposition. Finally, the perspectives for catalyst design for producing renewable hydrogen through the biogas reforming technology are presented.

KEYWORDS: biogas, carbon formation, catalyst deactivation, dry reforming of methane, hydrogen production.

1. INTRODUCTION

Biomass, particularly in Brazil, has received increasing attention as a renewable energy source. Due to Brazil's large territorial extension and strong agricultural activity, the byproducts of this industry are being studied for their potential in energy generation (Costa *et al.*, 2022). The biogas derived from the anaerobic decomposition of biomass, primarily composed of CH₄ and CO₂, has significant energy potential for producing renewable hydrogen (Yang *et al.*, 2014).

Hydrogen can be produced by reforming reactions, where methane reacts with water, carbon dioxide, or oxygen to produce syngas. Steam reforming is the conventional method for hydrogen production from hydrocarbons in the industry (Palma *et al.*, 2016). Dry reforming of methane (DRM - Eq. 1) is more appropriate for biogas upgrading due to its high CO₂ concentration and is a promising reaction for hydrogen production while mitigating greenhouse gas emissions. The main limitation of DRM technology remains catalyst deactivation caused by carbon deposition, metal sintering, or metal oxidation under reaction conditions. DRM, being an endothermic reaction ($\Delta H^\circ = 247$ kJ/mol), requires elevated reaction temperatures, thereby promoting many side reactions, notably CH₄ decomposition (Eq. 2); the Boudouard reaction (Eq. 3), which produces coke deposits over the catalyst surface; and the reverse water-gas shift (RWGS) (Eq. 4), which reduces the H₂ yield of the process (Bradford; Vannice, 1999).



The catalyst design for DRM reaction has been conducted using diverse approaches for supported metallic catalysts. Catalysts featuring noble metals like Pd, Pt, Rh, and others exhibit high activity and resistance to coke formation due to the low dissolution of carbon in their lattices. Nevertheless, the limited availability of noble metals in the environment has increased research into transition metals such as Ni. Although Ni activity is comparable to noble metals but with costs less, it is prone to coke formation due to its high CH₄ decomposition activity at high temperatures. Additionally, the Ni particle size directly affects the kinetics of CH₄ decomposition, in which larger particles favor the nucleation of carbon at the metal-support interface (Rostrup-Nielsen; Trimm, 1977).

The support plays a key role in preventing carbon formation in the DRM reaction. It can act in two strategies: (i) to increase the thermal stability of the material, avoiding the metal sintering at high temperatures, and (ii) to enhance the oxygen mobility of the support, promoting the rate of carbon gasification at the metal-support interface. A set of new strategies to synthesize Ni-based catalysts with low particle size has been adopted, such as the development of encapsulated metals into the support structure (Marinho *et*

al., 2020, 2021). The confined environment led to better thermal stability against metal sintering, in which the shell stabilizes the active metal in the catalyst due to the creation of a physical barrier between different metal particles. Furthermore, an increased interfacial area strengthens metal-support interaction, enhancing the catalytic performance (Marinho *et al.*, 2020, 2021).

Another strategy is the use of reducible supports, where the oxygen vacancies promote the carbon removal mechanism. The main example of this group of oxides is ceria (CeO_2), which can store and release oxygen depending on the environment, following a Mars-van Krevelen mechanism (Kambolis *et al.*, 2010). To optimize the oxygen vacancies on CeO_2 -based materials, solid solutions have been developed by inserting metal dopants, resulting in higher resistance to coke formation. Zr is the most used dopant for CeO_2 materials, responsible for promoting the mobility of oxygen species from bulk phase to surface (Bedrane; Descorme; Duprez, 2002) and enhancing the CeO_2 thermal stability (Hori *et al.*, 1998).

Following the recent advances in catalyst design for DRM reaction, this chapter will provide a detailed overview of the thermodynamics and mechanisms of DRM reaction. The focus is on the mechanism of carbon formation and the different strategies used in the Catalysis Group of the National Institute of Technology and the Federal University of Rio de Janeiro to develop catalysts resistant to carbon formation during DRM reaction conditions.

2. THERMODYNAMIC OF DRM REACTION

Figure 1 shows the equilibrium constant value of different reactions occurring simultaneously in the reactor during the DRM process as a function of temperature. The DRM reaction is very endothermic and thus occurs with high CH_4 conversion only at high temperatures. Nevertheless, these conditions promote methane decomposition, as demonstrated in Figure 1. The exothermic nature of the Boudouard reaction prevents its occurrence at high temperatures, while the thermodynamics limits the RWGS reaction above 1000 °C. As can be seen in Eqs. 1–4, carbon formation is attributed to methane decomposition and the Boudouard reaction. However, at high temperatures, only CH_4 decomposition is promoted, and this reaction has been associated with coke formation on Ni-based catalysts. Some efforts have been made to perform DRM at low temperatures to reduce operational costs; however, this condition favors the Boudouard reaction, acting as an additional source of coke on the catalyst.

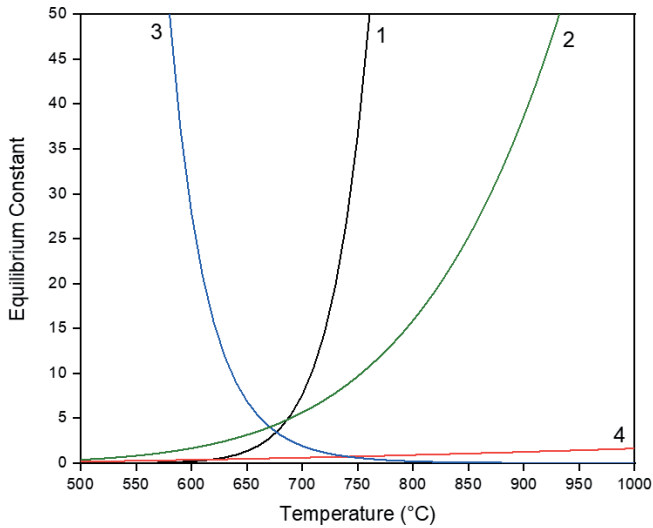


Figure 1 - Equilibrium constant of reactions as a function of reaction temperature: (1) DRM reaction, (2) CH₄ decomposition reaction, (3) Boudouard reaction, and (4) RWGS reaction.

The conversion of CH₄ and CO₂ as a function of temperature for different CH₄/CO₂ molar ratios for the DRM reaction is shown in Figure 2. The conversion increases with the rise in temperature for both reactants due to the endothermicity of the DRM reaction. A CH₄/CO₂ molar ratio exceeding 1.0 favors the CH₄ decomposition reaction, leading to an increase in the H₂/CO molar ratio. However, excess of CH₄ in the gas feed leads to a decrease in the CH₄ conversion and an increase in CO₂ conversion, acting as a limiting reactant in the reactor. Some experimental data have demonstrated high carbon formation derived from CH₄ decomposition on Ni-based catalysts using a feed composition with a CH₄/CO₂ molar ratio higher than 1.0 (Serrano-Lotina; Daza, 2014). Introducing more CO₂ into the feed increases the CH₄ conversion and decreases the CO₂ conversion, highlighting CH₄ acting as a limiting reactant. Furthermore, the H₂/CO molar ratio decreases due to the shifting of the RWGS reaction to the production of CO in an excess of CO₂.

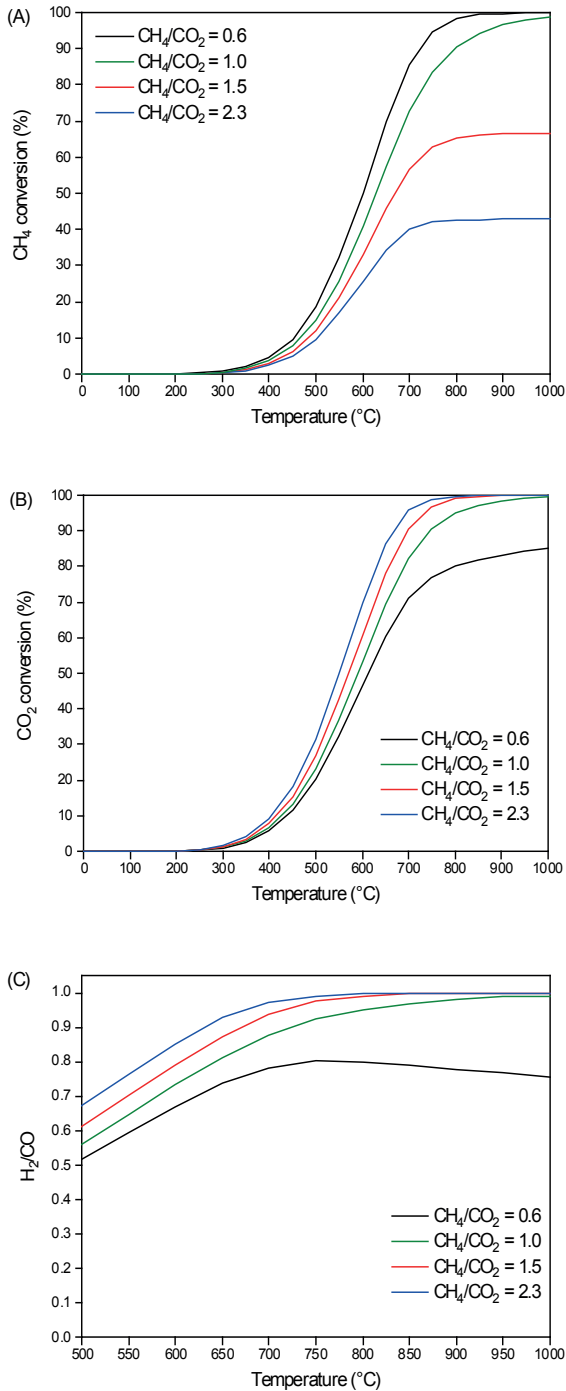


Figure 2 - (A) CH_4 conversion; (B) CO_2 conversion; (C) H_2/CO molar ratio obtained in the DRM reaction as a function of temperature at equilibrium condition.

The use of biogas for the DRM reaction is challenging since the CH₄/CO₂ molar ratio is close to 1.5, promoting a higher rate of carbon formation in equilibrium conditions. Thus, the design of catalysts resistant to coke formation, even under conditions favorable to carbon deposition, is desired for an effective process.

3. REACTION MECHANISM

An ideal catalyst for the DRM reaction is supposed to exhibit both high activity and stability under reaction conditions. Thus, a fundamental criterion for catalyst selection is its ability to decrease or suppress the rate of carbon formation. To achieve this, the mechanism for CH₄ and CO₂ activation in various catalytic systems must be considered (Papadopoulou; Matralis; Verykios, 2012). The mechanism of the DRM reaction has been studied for years as new techniques have been developed for its determination. The consensus in the literature is that methane adsorbs onto the metal surface before the reaction occurs, and the cleavage of the first C-H bond is considered the rate-determining step of the reaction (Wei; Iglesia, 2004). Therefore, the dissociated carbon remains adsorbed on the metallic crystallite. The adsorption of CO₂ can occur on the metal surface as well as on the support, depending on the type of metal and support. The activation of CO₂ is a crucial step as it is responsible for increasing the concentration of reactive oxygen species, thereby enhancing the rate of carbon gasification present in the metallic phase.

A. Methane Activation:

The initial stage involves the adsorption of CH₄ in a dissociative form onto the Ni sites. Methane adsorbs on a metallic site (Eq. 5), followed by successive dehydrogenation steps toward the formation of reactive carbon (Eqs. 6–9).



B. Carbon Dioxide Activation:

CO₂ may adsorb dissociatively on the metal as well as on the support. CO₂ adsorption on the support leads to the formation of carbonate and bicarbonate species (Eq. 10). In the case of reducible supports, CO₂ adsorbs on the oxygen vacancies, producing lattice oxygen OL and CO (Eq. 11). Therefore, CO₂ replenishes the oxygen vacancies of the support, releasing CO. The lattice oxygen species thus generated may react with C* produced from methane activation (Eq. 12), promoting the removal of carbon from the surface of metal particles, producing CO (Eq. 13). This redox mechanism is characteristic of lanthanides

or rare-earth metals and the most studied support is CeO₂. In its ideal stoichiometric state, each O²⁻ ion is coordinated by four Ce⁴⁺ ions. However, under reducing conditions, specifically in a H₂-rich atmosphere, oxygen is liberated from the CeO₂ lattice, leading to the formation of oxygen vacancies and the generation of Ce³⁺. The redox property results in high oxygen mobility to CeO₂ via a redox cycle between Ce⁴⁺/Ce³⁺ under the Mars-van Krevelen mechanism (Liew; Jalil; Tan, 2022).



4. MECHANISM OF CARBON FORMATION

The main reactions responsible for the formation of carbon during dry methane reforming are the methane decomposition reaction (Eq. 2) and the Boudouard reaction (also called the CO disproportionation reaction) (Eq. 3). Bengaard *et al.* (2002) proposed that carbon nucleation occurs at the step sites of nickel crystallites. The mechanism of carbon formation in methane reforming reactions is shown in Figure 3 (Trimm, 1997). Initially, the alpha carbon species (C_α) is formed, which is reactive and can be rapidly gasified to CO. However, if the rate of formation of this carbon is much greater than the rate of the gasification reaction, the C_α polymerizes, generating a new species of carbon called beta carbon (C_β). This new species has low reactivity under the reaction conditions and will be deposited on the catalyst. Two processes can occur with an excess of C_β on the catalyst surface:

(i) The encapsulation of the metallic surface, leading to total deactivation of the metallic site;

(ii) Dissolution in the crystallite of Ni, followed by its diffusion and precipitation at the rear of the crystallite, leading to the formation of carbon filaments. Figure 4 illustrates the formation of carbon nanotubes in Ni-based catalysts (Helveg *et al.*, 2011). This is the most common case in Ni-based catalysts. In this case, the formation of carbon does not lead to immediate deactivation of the catalyst, as the Ni particle located at the tip of the filament remains available for the reaction. However, the formation of carbon filaments will lead to increased pressure in the catalyst bed due to catalyst fragmentation and the need for catalyst replacement.

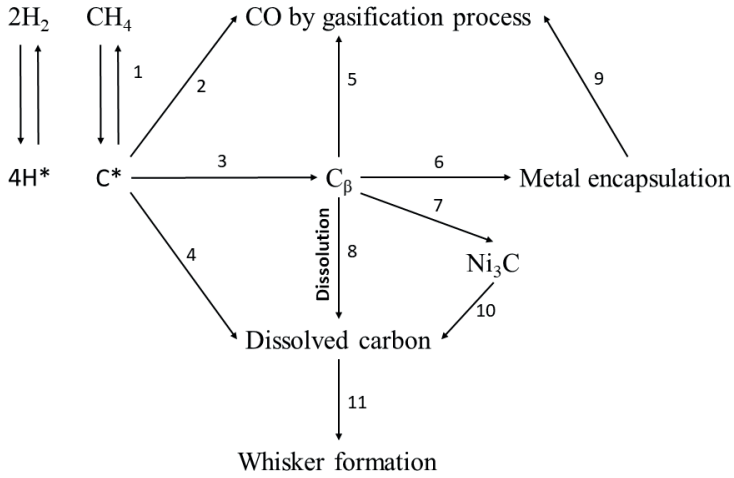


Figure 3 - Mechanism of carbon formation in methane reforming reaction (TRIMM, 1997).

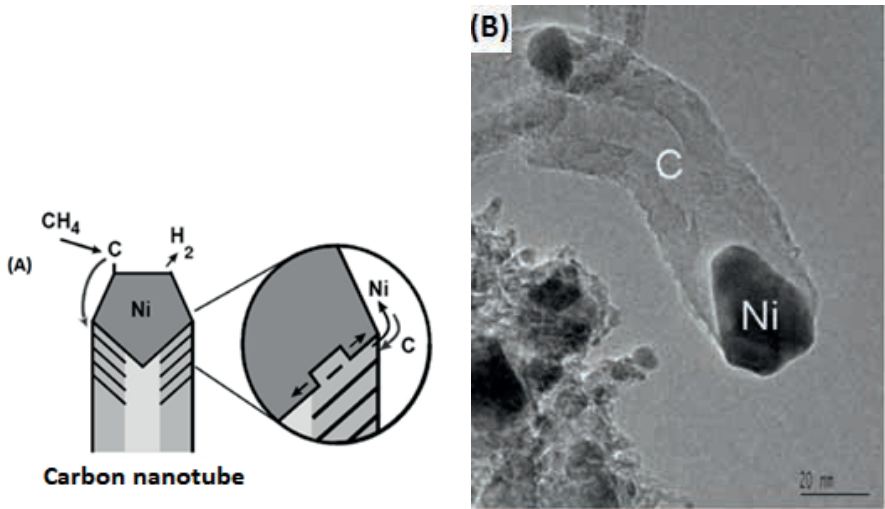
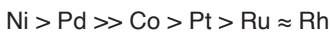


Figure 4 - (A) Scheme of the carbon formation mechanism, especially based on Ni; (B) Transmission electron microscopy image of carbon nanotube (Helveg; Sehested; Rostrup-Nielsen, 2011; Kehlet *et al.*, 2006).

This mechanism explains the low carbon formation on noble metals-based catalysts, as the solubility of carbon in these is much lower than in transition metals. Comparing the tendency of carbon formation during DRM on a series of transition metals supported on Al_2O_3 stabilized with MgO at 500–650 °C and 1 bar, Rostrup-Nielsen and Bak Hansen (1993) found the following order for carbon formation:



5. STRATEGIES FOR MINIMIZING CARBON FORMATION

Carbon formation may be minimized by controlling the rates of carbon nucleation and its gasification. The different strategies proposed to reduce or eliminate carbon formation include (i) controlling the size of the metallic crystallite and (ii) using supports with redox properties.

The CH_x species produced by the decomposition of CH_4 can undergo further dissociation to C and H. According to Trimm (1997), the dissociation of methane requires a defined number of atoms. Rostrup-Nielsen (1977) proposed a critical number of atoms below which carbon formation does not occur. Steam reforming requires ensembles of 3–4 atoms, while carbon formation needs 6–7 atoms. Therefore, the size of the nickel particle significantly influences the rate of carbon nucleation. The initiation step of carbon formation is more difficult at small particle sizes (Helveg *et al.*, 2011). Controlling particle size is a strategy for reducing or suppressing the rate of coke formation. Thus, selecting the catalyst preparation method is essential to control the size of the metallic particles and, consequently, the stability of the catalysts in the dry methane reforming reaction.

The catalyst synthesis method must lead to the formation of small and stable metallic particles. This can be achieved by methods that promote the interaction between the metal and the support. However, depending on the characteristics of the support, the reduction of metal oxides (e.g., especially Ni and Co oxides) may be difficult due to the strong interaction with the support. The formation of non-reducible mixed oxides, such as nickel aluminate, during the calcination or activation steps can also hinder reduction. The presence of these phases can result in loss of activity because the metal is considered the active site for the dry reforming of methane reaction. Therefore, appropriate preparation method that minimizes carbon formation has to be a compromise between obtaining small metal particles and the reducibility of the metal oxide. The different catalyst preparation methods proposed to obtain highly dispersed metallic particles include (i) sol-gel; (ii) the incorporation of metallic particles within the microporous and mesoporous channels of materials such as zeolites and SBA-15; (iii) the confinement of metallic particles in a core-shell structure; and (iv) the use of supports that promote the dispersion of the active phase.

Another approach consists of increasing the carbon gasification rate employing supports with high oxygen mobility, which can alternate the oxidation state of the metal present in the oxide to donate and receive oxygen in its structure. This strategy is based on the role of the support in the methane dry reforming reaction mechanism.

The decomposition of CH_4 and the dissociation of CO_2 occur via two independent pathways (Figure 5) (Stagg-Williams *et al.*, 2000; Noronha *et al.*, 2001; Rabelo-Neto *et al.*, 2018). The first path involves the decomposition of CH_4 on the metal particle, resulting in the formation of hydrogen and carbonaceous deposits. The carbon formed can partially reduce the support near the metal particle, producing CO. In the presence of an irreducible support,

carbon deposits remain on the surface, leading to catalyst deactivation. The second path is the dissociative adsorption of CO_2 onto the support, producing CO and oxygen. This oxygen replenishes oxygen vacancies, establishing a continuous cleaning redox mechanism. The balance between the methane decomposition rate and the cleaning rate determines the stability of the catalyst. In this two-way mechanism, the role of support is very important because it participates in the dissociative adsorption of CO_2 near metal particles, transferring oxygen to the surface of the metal particle containing carbon deposits, thus promoting the mechanism that removes carbon from the metal.

Cerium oxide has a high oxygen exchange capacity due to its ability to easily change its oxidation state, which leads to the formation of oxygen vacancies. Considering that the presence of oxygen vacancies close to the perimeter of the metallic particle is fundamental to the cleaning mechanism, one approach to improving the stability of the catalyst is to increase the reducibility of the support. This can be done by doping the ceria with different metals, such as zirconia. Therefore, the addition of zirconium oxide to ceria increases its reducibility and oxygen transfer capacity from the support by formation of a ceria-zirconia solid solution. Next, different examples of catalytic systems developed for the dry methane reforming reaction will be presented, aiming to obtain catalysts that are more resistant to deactivation.

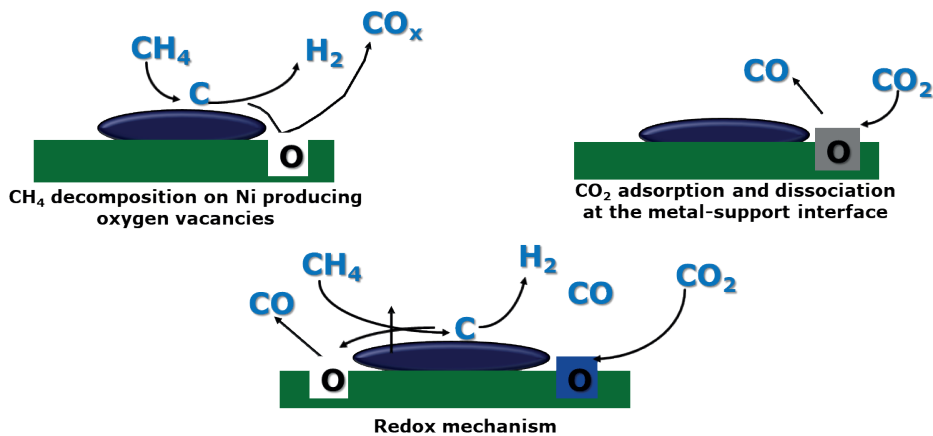


Figure 5 - Scheme for the dual path mechanism for DRM over Ni supported on ceria and ceria mixed oxides (Rabelo-Neto *et al.*, 2018).

6. DEVELOPMENT OF CATALYSTS RESISTANT TO CARBON FORMATION IN DRM

Da Fonseca *et al.* (2022) investigated the effect of Ni crystallite size and oxygen vacancies of the support on carbon formation over Ni/CeO_2 catalysts for the DRM at 1073 K. A large range of crystallite size was achieved using different Ni contents (5 and 10

wt%) and calcination temperatures (673, 873, 1073, and 1473 K). *In situ* XRD and XANES experiments at the L_{III} edge of Ce revealed that the increase in calcination temperature caused an increase in Ni crystallite size, while the amount of oxygen vacancies decreased. The Ni/CeO₂ catalysts were tested for the DRM at 1073 K for 24 h. Bulk NiO was also used as a reference. The 5Ni/CeO₂₋₆₇₃, 10Ni/CeO₂₋₆₇₃, 10Ni/CeO₂₋₈₇₃, and 10Ni/CeO₂₋₁₀₇₃ catalysts suffered a small drop in conversion over the 24 h of time on stream (TOS), while a higher loss of activity was observed at the beginning of the reaction for the 10Ni/CeO₂₋₁₄₇₃ and bulk NiO. Scanning electron microscopy images of the catalysts after the reaction revealed the presence of carbon filaments in the catalysts calcined at 673 and 1073 K, with the formation of carbon nanotubes not being observed in the 10Ni/CeO₂₋₁₄₇₃ and bulk NiO catalysts. The rate of carbon formation was determined through temperature-programmed oxidation (TPO) of the spent catalysts. The carbon formation rate (mgC/(gcat.h)) followed the order: 10Ni/CeO₂₋₆₇₃ (20.9) > 10Ni/CeO₂₋₈₇₃ (10.6) > 10Ni/CeO₂₋₁₀₇₃ (5.9) > 5Ni/CeO₂₋₆₇₃ (1.6) > 10Ni/CeO₂₋₁₄₇₃ (0.3) ≈ NiO (0.2). Figure 6 shows the variation of the carbon formation rate for the Ni/CeO₂ catalysts after the DRM reaction at 1073 K for 24 h as a function of the Ni crystallite size. The rate of carbon formation increased as the Ni crystallite size increased, reaching a maximum of around 20–30 nm and then continuously decreasing to 133 nm. Therefore, there is a critical size of the Ni crystallite for carbon formation during the DRM reaction over Ni/CeO₂ catalysts, in which the maximum amount of carbon is formed. Figure 6 illustrates the window for carbon formation during DRM, as carbon deposition below 10 nm and above 100 nm is negligible. For catalysts with very large Ni⁰ crystallite sizes (10Ni/CeO₂₋₁₄₇₃ and bulk NiO), the CH₄ dissociation rate was probably so low that the carbon species formed react, and carbon accumulation does not occur. Furthermore, supports with redox properties such as ceria play a fundamental role in the DRM reaction, participating in the mechanism of carbon removal from the metal surface (Figure 3). However, the effectiveness of the carbon removal mechanism also depends on the metal-support interaction and, thus, on the size of the metal particle. A larger metal-support interface favors the oxygen migration from the support to the metal surface, thus eliminating or reducing carbon accumulation. Therefore, this mechanism is promoted in highly dispersed metallic particles on supports with redox properties, such as ceria or mixed oxides ceria-zirconia. Then, the higher amount of oxygen vacancies of the cerium oxide support calcined at 673 K and the smaller Ni crystallite size on the 5Ni/CeO₂₋₆₇₃ catalyst led to a lower carbon formation rate. Increasing the Ni crystallite size to 20 nm reduced the metal-support interface and increased the rate of carbon formation. For the 10Ni/CeO₂₋₆₇₃ catalyst, the oxygen transfer rate from the support to the metal surface was insufficient to counterbalance the methane decomposition rate, and carbon accumulates on the surface despite the large number of oxygen vacancies observed in this catalyst. For the 10Ni/CeO₂₋₁₄₇₃ catalyst, the large crystallite size probably led to a low methane decomposition rate, in which the carbon species formed had time to react with CO₂ in the feed, preventing

carbon deposition even on a support with low oxygen vacancy density.

The so-called core-shell catalysts represent a strategy for controlling the size of metal particles and has been extensively studied. Core-shell catalysts are classified according to their composition, morphology, properties, and applications. The current classification of its morphology is much broader, as shown in Figure 7 (Das *et al.*, 2020).

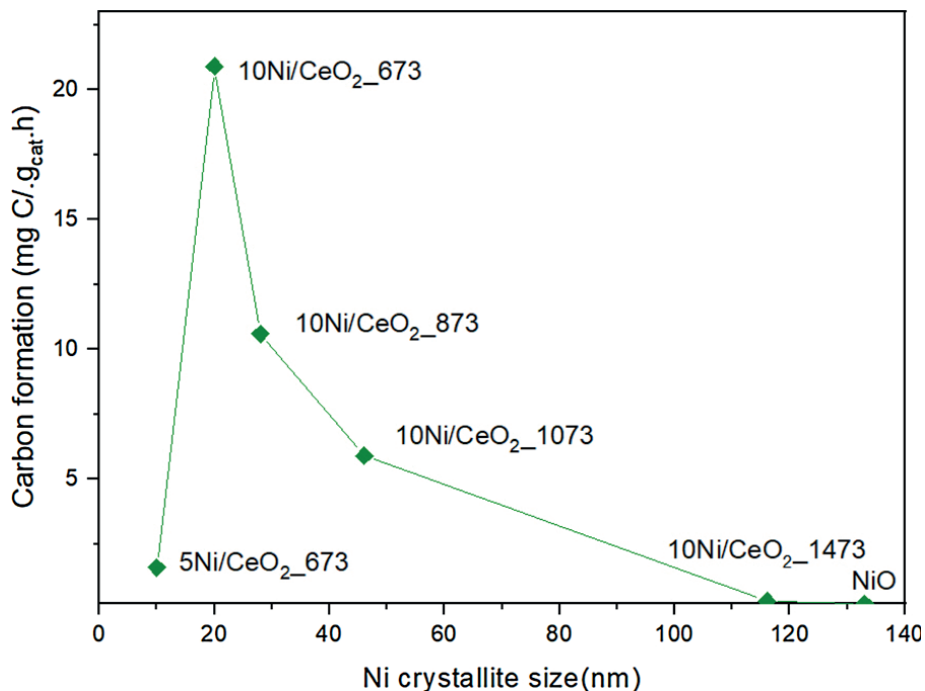


Figure 6 - Rate of carbon formation in the DRM reaction during 24 h of TOS as a function of Ni crystallite size. (Da Fonseca *et al.* (2022)).

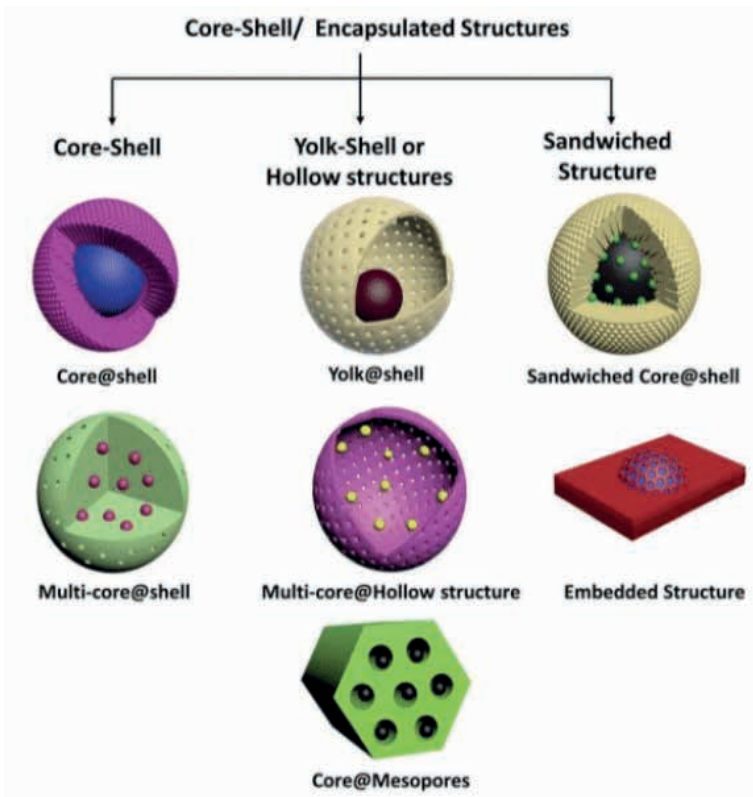


Figure 7 - Types of core-shell structures based on morphology (Das *et al.*, 2020).

Ni nanoparticles embedded in CeO_2 (Ni@CeO_2) and CeZrO_2 (Ni@CeZrO_2) were synthesized by sol-gel method and compared with a Ni/CeO_2 prepared by support impregnation (Marinho *et al.*, 2020). The performance of the catalysts was investigated for DRM reaction. The TEM images of the reduced Ni/CeO_2 , Ni@CeO_2 , and Ni@CeZrO_2 catalysts are shown in Figure 8. For the Ni/CeO_2 catalyst, the TEM image displays large Ni particles segregated on the surface of the sample, with an average particle size of around 30 nm. The TEM image of Ni@CeO_2 and Ni@CeZrO_2 catalysts reveals the presence of small Ni nanoparticles embedded in the ceria matrix formed during reduction. Segregated Ni particles could not be observed on the TEM images of Ni@CeO_2 and Ni@CeZrO_2 catalysts. Ni-embedded catalysts presented smaller metal particles than Ni/CeO_2 . For Ni@CeO_2 and Ni@CeZrO_2 , the Ni particle sizes were around 13 and 6 nm, respectively. Therefore, TEM found that Ni embedded in CeO_2 improved the resistance to sintering along the reduction at 800 °C. *In situ* XANES and XRD experiments showed that the embedded Ni particles in the ceria matrix were more difficult to reduce than the segregated particles characteristic of the impregnated catalyst. The strong interaction between Ni and CeO_2 improved the dispersion and avoided metal sintering at high temperatures. More oxygen vacancies were also generated on the catalysts containing Ni nanoparticles embedded in the support, as

demonstrated by the isotopic exchange experiments. The initial CH_4 and CO_2 conversions were approximately the same for all catalysts and remained quite constant during 24 h of TOS. Figure 8 shows TEM images of spent catalysts. The image of the Ni/CeO_2 catalyst exhibits the presence of Ni nanoparticles located inside the carbon filaments. For the $\text{Ni}@/\text{CeO}_2$ catalyst, TEM images reveal the presence of Ni nanoparticles into the bulk of CeO_2 , but sintering is observed (Ni particle size around 20 nm). This higher interaction inhibits the detachment of Ni particles from CeO_2 and the growth of carbon filament. The TEM images of $\text{Ni}@/\text{CeZrO}_2$ show Ni nanoparticles embedded into a ceria matrix with very small particle sizes (around 8 nm) after 24 h of TOS. Furthermore, carbon filaments were not observed, which demonstrated that inhibiting Ni sintering in the presence of a support with oxygen mobility suppressed the formation of carbon filaments. The rate of carbon formation was calculated through TG analysis of the used catalyst. Ni/CeO_2 catalyst exhibited the highest amount of carbon deposits ($9.7 \text{ mg}_C/(\text{g}_{\text{cat}}\cdot\text{h})$) but the carbon formation rate was significantly reduced for the catalysts containing Ni nanoparticles embedded in the ceria structure. For the $\text{Ni}@/\text{CeO}_2$ catalyst, the carbon formation rate was $1.6 \text{ mg}_C/(\text{g}_{\text{cat}}\cdot\text{h})$ whereas the $\text{Ni}@/\text{CeZrO}_2$ catalyst did not show evidence of carbon formation after DRM reaction. Therefore, the control of Ni particle size and the high oxygen mobility of the $\text{Ni}@/\text{CeZrO}_2$ catalyst inhibited carbon deposition and favored the mechanism of carbon removal, promoting catalyst stability.

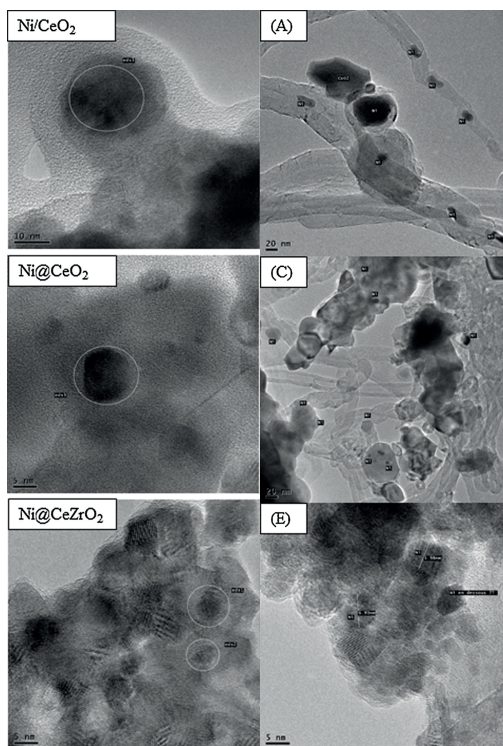


Figure 8 - TEM images of Ni/CeO_2 , $\text{Ni}@/\text{CeO}_2$, and $\text{Ni}@/\text{CeZrO}_2$ catalysts before and after DRM reaction at $800 \text{ }^\circ\text{C}$ for 24 h of TOS. (Marinho et al. (2020)).

The perovskite-type oxide (ABO_3) is an interesting class of material. These mixed oxides can produce very small metal particles upon reduction (Lima *et al.*, 2006; Valderrama *et al.*, 2005). Therefore, carbon formation could be decreased or inhibited on these highly dispersed metal particles. However, unsupported perovskite-type oxides have a low surface area, impacting their activity. One solution is to support the perovskite-type oxides on a high surface area oxide. Rabelo-Neto *et al.* (2018) deposited a perovskite-type oxide ($LaNiO_3$) over alumina and silica doped-ceria supports and tested them for the DRM reaction at 800 °C. Supported Ni catalysts were prepared by reducing $LaNiO_3$ perovskite precursors, producing Ni/La_2O_3 . The stability of the unsupported $LaNiO_3$, $LaNiO_3/Al_2O_3$, and $LaNiO_3/SiCeO_2$ catalysts for the DRM reaction at 800 °C was evaluated for 24 h. However, the test with the unsupported $LaNiO_3$ catalyst was stopped after 10 h due to a strong increase in pressure in the catalytic bed. For the $LaNiO_3/Al_2O_3$ catalyst, the CH_4 and CO_2 conversions increased and stabilized after 4 h of reaction (Figure 9). The performance of the $LaNiO_3/SiCeO_2$ catalyst was quite different. In this case, methane and CO_2 conversions increased only slightly during the first 6 h of reaction and then remained constant during 24 h. The higher CO_2 conversion than methane conversion, H_2/CO ratio values less than 1.0, and water formation were probably due to the RWGS. This behavior, i.e., the increase in CH_4 and CO_2 conversions at the beginning of the DRM reaction, was also observed in the literature and attributed to the oxidation of metallic particles by CO_2 in the feed. Then, the synthesis gas produced during the DRM reaction reduces the NiO particles formed, generating metallic Ni particles and increasing the conversion of CH_4 and CO_2 (Faria *et al.*, 2014; Takanabe *et al.*, 2005). To study the oxidation state of Ni during the DRM reaction, *in situ* XPS experiments were carried out. The intensity of the band corresponding to the binding energy of Ni 3p at 66 eV decreases continuously during the reaction in the $LaNiO_3/Al_2O_3$ catalyst while it remained approximately constant in the $LaNiO_3/SiCeO_2$. These results confirm the oxidation of metallic Ni particles by CO_2 in the feed at the beginning of the DRM reaction for the $LaNiO_3/Al_2O_3$ catalyst. TG analyses of the used catalysts were performed to investigate carbon formation. The TPO profiles of the $LaNiO_3$ and $LaNiO_3/Al_2O_3$ catalysts showed peaks at 625 and 643 °C, respectively, while no peak was observed in the TPO profile of the $LaNiO_3/SiCeO_2$ catalyst. These results demonstrated the formation of carbon filaments in the bulk and alumina-supported $LaNiO_3$ catalysts. The largest amount of carbon was formed on unsupported $LaNiO_3$. Supporting the $LaNiO_3$ phase significantly decreased the amount of carbon deposited. For alumina, the amount of carbon was approximately one third of that for the unsupported $LaNiO_3$. The deposition of $LaNiO_3$ on $SiCeO_2$ practically eliminated carbon formation. The operando XPS experiments showed the presence of a high fraction of Ce^{3+} species during the reaction, demonstrating that the redox cycle (Figure 5) was operational during the DRM reaction on the $LaNiO_3/SiCeO_2$ catalyst, which contributed to the removal of carbon deposits, promoting catalyst stability. Furthermore, *in situ* XRD measurements showed that the metal-ceria interaction also inhibited metal sintering during the reaction.

The growth of Ni crystallite size during DRM was lower in the $\text{LaNiO}_3/\text{SiCeO}_2$ catalyst, which also contributed to the lower carbon formation.

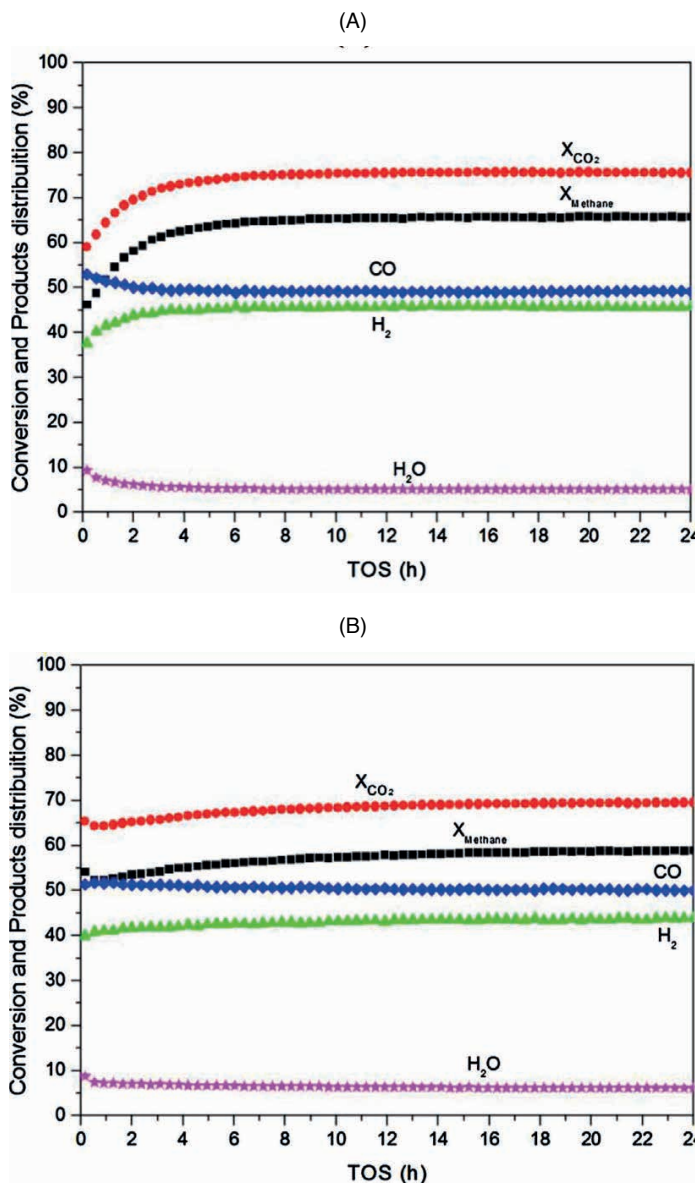


Figure 9 - CH_4 and CO_2 conversion and product distribution for DRM at 800 °C for 24 h of TOS over: (A) $\text{LaNiO}_3/\text{Al}_2\text{O}_3$; (B) $\text{LaNiO}_3/\text{SiCeO}_2$. (Rabelo-Neto et al. (2018)).

In addition to the perovskite-type oxides, the spinel phase has also been used to control Ni sintering during reduction at high temperatures, providing a high metal dispersion on the catalyst (Xu *et al.*, 2001). The Evaporation Induced Self-Assembly (EISA) method was

used to obtain highly dispersed Ni particles due to the formation of NiAl_2O_4 spinel structure (Marinho *et al.*, 2021). The high dispersion of Ni results from the reduction of NiAl_2O_4 , as observed from the XRD experiments, which prevents sintering at high temperatures. After reduction, small-size metallic Ni particles were observed (< 5 nm) for the catalyst prepared by EISA (10-Ni-CeAl). The catalyst synthesized by traditional impregnation of CeAl support exhibited a larger Ni crystallite size (11.3 nm). The 10Ni-Al and 5Ni-CeAl catalysts exhibited low initial CH_4 and CO_2 conversions that significantly increased during the first 2 h of TOS, and then they leveled off. For the 10Ni-CeAl and 10Ni/CeAl catalysts, the CH_4 and CO_2 conversions remained constant from the beginning of the reaction. However, the test was interrupted after 24 h of TOS for the 10Ni/CeAl catalyst due to the significant increase in the pressure drop on the reactor. The induction period observed for the 10Ni-Al and 5Ni-CeAl catalysts was attributed to the oxidation of Ni particles by CO_2 when the catalysts are initially contacted with the feed, resulting in a loss of activity. Nevertheless, the partially oxidized Ni particles were reduced again by the syngas produced during the reaction, increasing the conversion of reactants. The spent catalysts were characterized by TEM and TG analyses to investigate the formation of carbon deposits. No carbon filaments are observed on the TEM images of the 10Ni-CeAl catalyst. The average Ni particle size is around 10 nm, which indicates a slight increase compared to the reduced sample (4–5 nm according to the XRD and TEM results). The TEM images of the 10Ni-Al and 10Ni/CeAl catalysts after the DRM reaction reveal high carbon formation, with the presence of many carbon filaments. The Ni particle size is higher than the ones observed for the 10Ni-CeAl catalyst (around 20 nm for both catalysts). TG analysis did not detect carbon deposits on the 5Ni-CeAl and 10Ni-CeAl catalysts prepared by the EISA method. However, carbon was formed over the catalyst prepared by impregnation (10/Ni/CeAl: 2.0 mgC/(gcatal.h)). The presence of Ce in the structure increased the oxygen mobility and acted as sites for CO_2 adsorption, promoting the carbon removal mechanism. Therefore, the Ni-based CeO_2 - Al_2O_3 catalysts prepared by the one-pot EISA method exhibited high activity and stability for the DRM due to the confinement of Ni particles and the inhibition of carbon deposition by the Ce in the structure.

Table 1 summarizes the rate of carbon deposition during DRM over different Ni-based catalysts from the literature and developed in the Catalysis group of the National Institute of Technology (INT). The different strategies used to develop catalysts resistant to carbon deposition were successful.

Table 1 - Rate of carbon formation on Ni-based catalysts from the literature after DRM.

Catalyst	Reaction Conditions	Rate of carbon deposition ($\text{mg}_C/\text{g}_{\text{catal}}/\text{h}$)	Reference
5Ni-CeAl	800 °C, $\text{CH}_4:\text{CO}_2 = 1:1$	0.0	(Marinho <i>et al.</i> , 2021)
10Ni-CeAl	800 °C, $\text{CH}_4:\text{CO}_2 = 1:1$	0.0	(Marinho <i>et al.</i> , 2021)
10Ni/CeAl	800 °C, $\text{CH}_4:\text{CO}_2 = 1:1$	2.0	(Marinho <i>et al.</i> , 2021)
10Ni-Al	800 °C, $\text{CH}_4:\text{CO}_2 = 1:1$	0.8	(Marinho <i>et al.</i> , 2021)
Ni/CeO ₂	800 °C, $\text{CH}_4:\text{CO}_2 = 1:1$	9.7	(Marinho <i>et al.</i> , 2020)
Ni@CeO ₂	800 °C, $\text{CH}_4:\text{CO}_2 = 1:1$	1.6	(Marinho <i>et al.</i> , 2020)
Ni@CeZrO ₂	800 °C, $\text{CH}_4:\text{CO}_2 = 1:1$	0.0	(Marinho <i>et al.</i> , 2020)
LaNiO ₃	800 °C, $\text{CH}_4:\text{CO}_2 = 1:1$	27.0	(Rabelo-Neto <i>et al.</i> , 2018)
LaNiO ₃ /SiCeO ₂	800 °C, $\text{CH}_4:\text{CO}_2 = 1:1$	0.3	(Rabelo-Neto <i>et al.</i> , 2018)
Ni/0Ce-AlO	800 °C, $\text{CH}_4:\text{CO}_2 = 1:1$	3.7	(Chen <i>et al.</i> , 2013)
Ni/05CeAlO	800 °C, $\text{CH}_4:\text{CO}_2 = 1:1$	2.8	(Chen <i>et al.</i> , 2013)
Ni/10CeAlO	800 °C, $\text{CH}_4:\text{CO}_2 = 1:1$	1.8	(Chen <i>et al.</i> , 2013)
Ni/15CeAlO	800 °C, $\text{CH}_4:\text{CO}_2 = 1:1$	1.2	(Chen <i>et al.</i> , 2013)
NiCu/Ce _{0.9} Gd _{0.1} O ₂	800 °C, $\text{CH}_4:\text{CO}_2 = 1:1$	12.2	(Bonura; Cannilla; Frusteri, 2012)
Ni/CeO ₂	800 °C, $\text{CH}_4:\text{CO}_2 = 1:1$	4.8	(Luisetto <i>et al.</i> , 2019)
Ni/CZ100	700 °C, $\text{CH}_4:\text{CO}_2 = 1:1$	0.4	(Kambolis <i>et al.</i> , 2010)
Ni/CZ75	700 °C, $\text{CH}_4:\text{CO}_2 = 1:1$	3.5	(Kambolis <i>et al.</i> , 2010)
Ni/CZ44	700 °C, $\text{CH}_4:\text{CO}_2 = 1:1$	1.7	(Kambolis <i>et al.</i> , 2010)
Ni/CZ28	700 °C, $\text{CH}_4:\text{CO}_2 = 1:1$	0.7	(Kambolis <i>et al.</i> , 2010)
Ni/CeZr(8.5)	700 °C, $\text{CH}_4:\text{CO}_2 = 1:1$	15	(Donphai <i>et al.</i> , 2023)
20Ce/Ni@SiO ₂	700 °C, $\text{CH}_4:\text{CO}_2 = 1:1$	2.2	(Zhou <i>et al.</i> , 2022)
Ni/Ce _{0.95} Zr _{0.05} O ₂	800 °C, $\text{CH}_4:\text{CO}_2 = 1:1$	0.0	(Zou <i>et al.</i> , 2023)

The carbon deposition in the DRM reaction strongly depends on the type of metal being used (Noronha *et al.*, 2001). In general, Group VIII metals are less prone to coking than Ni and Co, but their ability to operate with low carbon deposition in CO₂ reforming of methane is strongly related to their activity for CO₂ dissociation. For example, Ru and Rh are very active in CO₂ dissociation, and they can perform the CO₂ reforming of CH₄ without carbon deposition. Although the type of support used can affect the methane-reforming activity of metals like Ru or Rh, which are efficient for dissociating CO₂, those effects are much less crucial than in the case of Pt and Pd. This difference is due to the different abilities of the metals for CO₂ dissociation. A metal able to dissociate CO₂ can efficiently eliminate carbon produced by methane decomposition. In contrast, Pt or Pd require the assistance of the support to keep their surface free of carbon. Therefore, Pt supported on ceria and ceria mixed oxides catalysts have been extensively tested for DRM. However, ceria generally exhibits low surface area, which leads to low metal dispersion. A solution to overcome this problem is to deposit the ceria on high-area supports such as alumina (Azevedo *et al.*, 2022; Da Fonseca *et al.*, 2020a, 2020b).

Da Fonseca *et al.* (2020a) investigated how the nature of the dopant (Pr, Nb, and Zr) affects the performance of Pt supported on cerium-based oxides deposited on alumina for DRM. *In situ* XRD and XANES experiments showed that the catalyst doped with Pr achieved the highest reducibility of ceria (23%). Furthermore, the addition of Pr improved the resistance to metal sintering during the dry reforming reaction. The catalysts were tested for DRM at 800 °C for 24 h. For undoped catalyst (Pt/Al₂O₃), a strong deactivation occurred during the reaction due to the absence of support reducibility and the highest Pt sintering. However, adding Pr, Zr, and Nb to cerium oxide significantly decreased the loss of catalytic activity, mainly for the sample containing Pr. TPO analyses of the spent catalysts showed that the presence of dopants decreased carbon accumulation on the Pt surface. Moreover, for doped samples, a change of ceria oxidation states between Ce⁴⁺ and Ce³⁺ was observed during reduction treatment, as revealed by *in situ* XRD and XANES experiments. This effect was more significant for Pt/CePr/Al₂O₃, indicating that this sample presented the highest oxygen storage/release capacity, promoting the carbon removal mechanism from the metallic surface. In addition to carbon formation, metal sintering also occurred on the Pt/CeNb/Al₂O₃, Pt/CeZr/Al₂O₃, and especially the Pt/Al₂O₃ catalyst. The decrease in metal dispersion also contributed to the deactivation of these catalysts during DRM. Among the doped-ceria samples, Pt/CePr/Al₂O₃ exhibited the highest activity and stability. These results were attributed to (i) the oxygen mobility of the supports containing ceria, mainly for the sample doped with Pr, which favors the carbon removal mechanism, and (ii) the absence of Pt sintering during the reaction.

CONCLUSIONS AND PERSPECTIVES

Development of a biogas reforming technology is a potential route for hydrogen production in Brazil. Among the reforming processes, DRM benefits from using CO₂ as an oxidizing agent, decreasing associated costs to steam production with simultaneous CO₂ valorization. Despite its environmental promise, DRM technology has not yet reached industrial-scale operation, mainly because of the high coke formation and metal sintering, which occur in harsh reaction operations, leading to catalyst deactivation.

Research and development in this field are highly active, with Ni-based materials as one of the most common catalysts. Catalysts with small particles, often incorporating mixtures of elements (CeO₂ and Ce-doped materials), showed promising results in achieving high methane conversion and resistance to deactivation. The development of supports with high oxygen mobility promotes coke gasification during reaction. In addition, new catalyst structures with confined Ni nanoparticles have been developed to control the CH₄ decomposition. The development of such materials is crucial to highly dispersed Ni nanoparticles at high temperatures. The results showed that a balanced combination of well-dispersed metal on a support with high oxygen mobility could be a successful approach for DRM reaction.

Several key future research directions are top priorities in advancing biogas reforming technology:

1. **Tailoring of Metal-Support Interaction:** The rational design of DRM catalysts should focus on studying metal-support interaction. Parameters such as oxygen vacancies, oxygen mobility, and support-induced effects can significantly enhance the resistance against deactivation by coke formation or metal sintering.
2. **Advanced Synthesis Methods for Ni particle size control:** The utilization of advanced synthesis methods capable of fine-tuning the Ni crystallite size is crucial. This sintering control allows the design of DRM catalysts with remarkable resistance to coke formation. New studies should be conducted in this direction, such as developing single-atom catalysts.
3. **High-Pressure DRM Investigation:** Very few works have explored the development of catalysts to operate at high pressure during DRM reactions. Although high-pressure DRM has been considered to have lower costs than ambient pressure conditions, it has been relatively unexplored due to challenges such as enhanced coke formation, higher temperature requirements, and the formation of coke precursors. The catalyst design under high operating pressures is an important way to reduce costs in realistic DRM processes.
4. **Application of Advanced Operando Techniques:** DRM reaction occurs at high temperatures, and the catalyst can undergo changes during the reaction. Understanding the relationships between structure and activity at the atomic level is important to improve catalyst design techniques. Advanced *operando* techniques can be crucial in addressing the challenges outlined above. These techniques, including FTIR, XPS, or EXAFS spectroscopy, can provide valuable insights into the identity of key reaction intermediates, reaction pathways, and the effects of temperature and pressure on both mechanisms and coke formation on catalyst surfaces. Applying these techniques will contribute to a comprehensive understanding of variations in reaction mechanisms and kinetics of DRM reactions.

REFERENCES

AZEVEDO, I. R. *et al.* Long-term stability of Pt/Ce_{0.8}Me_{0.2}O₂-γ/Al₂O₃ (Me = Gd, Nb, Pr, and Zr) catalysts for steam reforming of methane. **International Journal of Hydrogen Energy**, v. 47, n. 35, p. 15624–15640, 26 Apr. 2022.

BEDRANE, S.; DESCORME, C.; DUPREZ, D. Investigation of the oxygen storage process on ceria- and ceria–zirconia-supported catalysts. **Catalysis Today**, Environmental Catalysis: a step forward. v. 75, n. 1, p. 401–405, 3 July 2002.

BENGAARD, H. S. *et al.* Steam Reforming and Graphite Formation on Ni Catalysts. **Journal of Catalysis**, v. 209, n. 2, p. 365–384, 25 July 2002.

BONURA, G.; CANNILLA, C.; FRUSTERI, F. Ceria–gadolinia supported NiCu catalyst: A suitable system for dry reforming of biogas to feed a solid oxide fuel cell (SOFC). **Applied Catalysis B: Environmental**, v. 121–122, p. 135–147, 13 June 2012.

- BRADFORD, M. C. J.; VANNICE, M. A. CO₂ Reforming of CH₄. **Catalysis Reviews**, v. 41, n. 1, p. 1–42, 2 Feb. 1999.
- CHEN, W. *et al.* High carbon-resistance Ni/CeAlO₃-Al₂O₃ catalyst for CH₄/CO₂ reforming. **Applied Catalysis B: Environmental**, v. 136–137, p. 260–268, 5 June 2013.
- COSTA, G. G. DA *et al.* Mapping and energy analysis of Brazilian bioenergy power potential for three agricultural biomass byproducts. **Journal of Cleaner Production**, v. 349, p. 131466, 15 May 2022.
- DA FONSECA, R. O. *et al.* Pt supported on doped CeO₂/Al₂O₃ as catalyst for dry reforming of methane. **International Journal of Hydrogen Energy**, 22nd World Hydrogen Energy Conference. v. 45, n. 8, p. 5182–5191, 14 Feb. 2020a.
- DA FONSECA, R. O. *et al.* Study of the effect of Gd-doping ceria on the performance of Pt/GdCeO₂/Al₂O₃ catalysts for the dry reforming of methane. **Catalysis Today**, SI: Energy and the Environment. v. 355, p. 737–745, 15 Sept. 2020b.
- DA FONSECA, R. O. *et al.* Controlling carbon formation over Ni/CeO₂ catalyst for dry reforming of CH₄ by tuning Ni crystallite size and oxygen vacancies of the support. **Journal of CO₂ Utilization**, v. 57, p. 101880, 1 Mar. 2022.
- DAS, S. *et al.* Core–shell structured catalysts for thermocatalytic, photocatalytic, and electrocatalytic conversion of CO₂. **Chemical Society Reviews**, v. 49, n. 10, p. 2937–3004, 26 May 2020.
- FARIA, E. C. *et al.* Hydrogen production through CO₂ reforming of methane over Ni/CeZrO₂/Al₂O₃ catalysts. **Catalysis Today**, Natural Gas Conversion the Status and Potentials in the Light of NGCS-10. v. 228, p. 138–144, 1 June 2014.
- HELVEG, S.; SEHESTED, J.; ROSTRUP-NIELSEN, J. R. Whisker carbon in perspective. **Catalysis Today**, v. 178, p. 42–46, 2011.
- HORI, C. E. *et al.* Thermal stability of oxygen storage properties in a mixed CeO₂-ZrO₂ system. **Applied Catalysis B: Environmental**, v. 16, n. 2, p. 105–117, 27 Mar. 1998.
- KAMBOLIS, A. *et al.* Ni/CeO₂-ZrO₂ catalysts for the dry reforming of methane. **Applied Catalysis A: General**, v. 377, n. 1, p. 16–26, 1 Apr. 2010.
- KEHLET, J. *et al.* Mechanisms for catalytic carbon nanofiber growth studied by ab initio density functional theory calculations. **Physical Review B (Condensed Matter and Materials Physics)**, v. 73, n. 11, 2006.
- LIEW, S. Y.; JALIL, A. A.; TAN, J. S. A short review on the promotional effects of ceria-based catalyst for dry reforming methane. **Journal of Physics: Conference Series**, v. 2259, n. 1, p. 012020, Apr. 2022.
- LIMA, S. M. *et al.* Structural features of La_{1-x}Ce_xNiO₃ mixed oxides and performance for the dry reforming of methane. **Applied Catalysis A: General**, v. 311, p. 94–104, 1 Sept. 2006.
- LUISETTO, I. *et al.* Dry reforming of methane over Ni supported on doped CeO₂: New insight on the role of dopants for CO₂ activation. **Journal of CO₂ Utilization**, v. 30, p. 63–78, 1 Mar. 2019.

MARINHO, A. L. A. *et al.* Embedded Ni nanoparticles in CeZrO₂ as stable catalyst for dry reforming of methane. **Applied Catalysis B: Environmental**, v. 268, p. 118387, 5 July 2020.

MARINHO, A. L. A. *et al.* Highly active and stable Ni dispersed on mesoporous CeO₂-Al₂O₃ catalysts for production of syngas by dry reforming of methane. **Applied Catalysis B: Environmental**, v. 281, p. 119459, 1 Feb. 2021.

NORONHA, F. B. *et al.* Correlation between catalytic activity and support reducibility in the CO₂ reforming of methane over Pt/Ce_xZr_{1-x}O₂ catalysts. **Chemical Engineering Journal**, FRONTIERS IN CHEMICAL REACTION ENGINEERING. v. 82, n. 1, p. 21–31, 15 Mar. 2001.

PALMA, V. *et al.* Experimental and numerical investigations on structured catalysts for methane steam reforming intensification. **Journal of Cleaner Production**, Special Volume: Process Integration for Cleaner Production. v. 111, p. 217–230, 16 Jan. 2016.

PAPADOPOULOU, C.; MATRALIS, H.; VERYKIOS, X. Utilization of Biogas as a Renewable Carbon Source: Dry Reforming of Methane. Em: GUCZI, L.; ERDŐHELYI, A. (Eds.). **Catalysis for Alternative Energy Generation**. New York, NY: Springer, 2012. p. 57–127.

PHICHAIRATANAPHONG, O.; DONPHAI, W. Role of Cerium–Zirconium Ratio and Chemical Surface Property of CeO₂-ZrO₂ Supported Nickel-Based Catalysts in Dry Reforming Reaction. **Topics in Catalysis**, 10 June 2023.

RABELO-NETO, R. C. *et al.* CO₂ reforming of methane over supported LaNiO₃ perovskite-type oxides. **Applied Catalysis B: Environmental**, v. 221, p. 349–361, 1 Feb. 2018.

ROSTRUPNIELSEN, J. R.; HANSEN, J. H. B. CO₂-Reforming of Methane over Transition Metals. **Journal of Catalysis**, v. 144, n. 1, p. 38–49, 1 nov. 1993.

ROSTRUP-NIELSEN, J.; TRIMM, D. L. Mechanisms of carbon formation on nickel-containing catalysts. **Journal of Catalysis**, v. 48, n. 1, p. 155–165, 30 June 1977.

SERRANO-LOTINA, A.; DAZA, L. Influence of the operating parameters over dry reforming of methane to syngas. **International Journal of Hydrogen Energy**, v. 39, n. 8, p. 4089–4094, 6 Mar. 2014.

TAKANABE, K. *et al.* Influence of reduction temperature on the catalytic behavior of Co/TiO₂ catalysts for CH₄/CO₂ reforming and its relation with titania bulk crystal structure. **Journal of Catalysis**, v. 230, n. 1, p. 75–85, 15 Feb. 2005.

TRIMM, D. L. Coke formation and minimisation during steam reforming reactions. **Catalysis Today**, Catalyst Deactivation by Coke Formation. v. 37, n. 3, p. 233–238, 15 Aug. 1997.

VALDERRAMA, G. *et al.* Dry reforming of methane over Ni perovskite type oxides. **Catalysis Today**, Selected Contributions of the XIX Ibero American Catalysis Symposium. v. 107–108, p. 785–791, 30 Oct. 2005.

WEI, J.; IGLESIA, E. Isotopic and kinetic assessment of the mechanism of methane reforming and decomposition reactions on supported iridium catalysts. **Physical Chemistry Chemical Physics**, v. 6, n. 13, p. 3754–3759, 9 July 2004.

XU, Z. *et al.* Bound-state Ni species — a superior form in Ni-based catalyst for CH₄/CO₂ reforming. **Applied Catalysis A: General**, v. 210, n. 1, p. 45–53, 9 Mar. 2001.

YANG, L. *et al.* Progress and perspectives in converting biogas to transportation fuels. **Renewable and Sustainable Energy Reviews**, v. 40, p. 1133–1152, 1 Dec. 2014.

ZHOU, Q. *et al.* Complete confinement of Ce/Ni within SiO₂ nanotube with high oxygen vacancy concentration for CO₂ methane reforming. **Fuel**, v. 325, p. 124819, 1 Oct. 2022.

ZOU, Z. *et al.* Preparing a Zr-Doped CeO₂ Nanorod to Improve the Catalytic Performance of the Ni-Based Catalyst for Dry Reforming of Methane by Enhancing Oxygen Supply. **ACS Sustainable Chemistry & Engineering**, v. 11, n. 19, p. 7443–7453, 15 May 2023.